

1 **NO₂-initiated multiphase oxidation of SO₂ by O₂ on CaCO₃ particles**

2 Ting Yu^{1,2,*}, Defeng Zhao^{1,2,*}, Xiaojuan Song^{1,2}, Tong Zhu^{1,2}

3 BIC-ESAT and SKL-ESPC, College of Environmental Sciences and Engineering, Peking University, Beijing,
4 100871, China

5 *These authors contributed equally to this work.

6 *Correspondence to:* Tong Zhu (tzhu@pku.edu.cn)

7 **Abstract.** The reaction of SO₂ with NO₂ on the surface of aerosol particles has been suggested to be important in
8 sulfate formation during severe air pollution episodes in China. However, we found that the direct oxidation of
9 SO₂ by NO₂ was slow and might not be the main reason for sulfate formation in ambient air. In this study, we
10 investigated the multiphase reaction of SO₂ with an O₂/NO₂ mixture on single CaCO₃ particles using
11 Micro-Raman spectroscopy. The reaction converted the CaCO₃ particle to a Ca(NO₃)₂ droplet, with CaSO₄•2H₂O
12 solid particles embedded in it, which constituted a significant fraction of the droplet volume at the end of the
13 reaction. The reactive uptake coefficient of SO₂ for sulfate formation was on the order of 10⁻⁵, which was higher
14 than that for the multiphase reaction of SO₂ directly with NO₂ by 2–3 orders of magnitude. According to our
15 observations and the literature, we found that in the multiphase reaction of SO₂ with the O₂/NO₂ mixture, O₂ was
16 the main oxidant of SO₂ and was necessary for radical chain propagation. NO₂ acted as the initiator of radical
17 formation, but not as the main oxidant. The synergy of NO₂ and O₂ resulted in much faster sulfate formation than
18 the sum of the reaction rates with NO₂ and with O₂ alone. We estimated that the multiphase oxidation of SO₂ by
19 O₂ initiated by NO₂ could be an important source of sulfate and a sink of SO₂, based on the calculated lifetime of
20 SO₂ regarding the loss through the multiphase reaction versus the loss through the gas-phase reaction with OH
21 radical. Parameterizing the reactive uptake coefficient of the reaction observed in our laboratory for further model
22 simulation is needed, as well as an integrated assessment based on field observations, laboratory study results,
23 and model simulations to evaluate the importance of the reaction in ambient air during severe air pollution
24 episodes, especially in China.

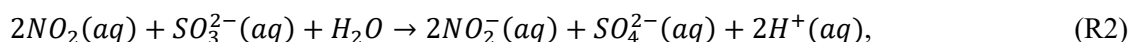
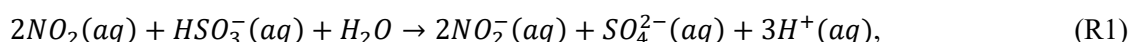
25 **1 Introduction**

26 It has been suggested that multiphase or heterogeneous oxidation of SO_2 potentially plays an important role
27 in sulfate formation in the atmosphere (Seinfeld and Pandis, 2006). During the severe pollution episodes that
28 occur frequently in China, high sulfate concentrations cannot be explained by the gas phase oxidation of SO_2 and
29 its well-known aqueous chemistry (Zheng et al., 2015a; Cheng et al., 2016), highlighting the role of
30 under-appreciated heterogeneous oxidation or multiphase pathways.

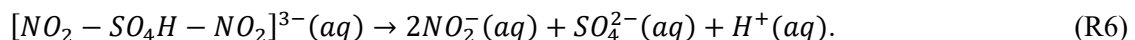
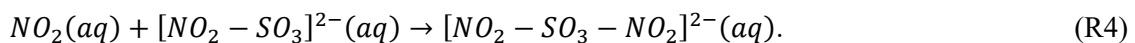
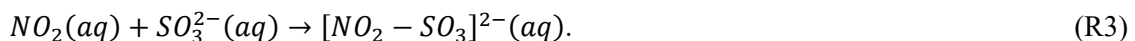
31 Recently, the multiphase oxidation of SO_2 by NO_2 has been introduced in air quality model simulations to
32 explain the discrepancy between the modeled and observed sulfate concentration during severe pollution episodes
33 in China (Cheng et al., 2016; Gao et al., 2016; Wang et al., 2016; Xue et al., 2016), despite the uncertainties in
34 the kinetic parameters for SO_2 oxidation and in the pH value of aerosol particles in China (Wang et al., 2016;
35 Cheng et al., 2016; Liu et al., 2017; Guo et al., 2017). However, according to our recently published results (Zhao
36 et al., 2017), the direct oxidation of SO_2 by NO_2 could not contribute significantly to sulfate formation in the
37 atmosphere because the reactive uptake coefficient of SO_2 for sulfate formation due to direct oxidation by NO_2 is
38 very low ($\sim 10^{-8}$).

39 Although the contribution of the direct oxidation of SO_2 by NO_2 to sulfate formation is not significant, NO_2
40 may be involved in other oxidation pathways of SO_2 . It has been reported that the reaction of NO_2 with SO_3^{2-} and
41 HSO_3^- in the bulk aqueous phase can form the $\text{SO}_3^{\cdot-}$ radical, which can further react with O_2 and produce a series
42 of radicals that oxidize S(IV) species (Littlejohn et al., 1993). The reaction pathway may result in a fast SO_2
43 oxidation due to the potential synergy of NO_2 and O_2 .

44 Despite such a reaction mechanism for SO_2 oxidation being proposed, its role in SO_2 oxidation in the
45 ambient atmosphere is not well established. Most previous studies have focused on the direct reaction of SO_2
46 with NO_2 , including the determination of its rate constant (Lee and Schwartz, 1983; Clifton et al., 1988; Shen and
47 Rochelle, 1998; Spindler et al., 2003; Nash, 1979; Huie and Neta, 1986). According to the reaction products and
48 their reported yields (Lee and Schwartz, 1983; Clifton et al., 1988), the overall reaction equations of the direct
49 reaction of SO_2 with NO_2 are as follows:



52 and the reactions are proposed to proceed via NO_2 -S(IV) adduct complexes (Clifton et al., 1988).



57 However, studies of the oxidation rate of SO_2 at the O_2 concentrations relevant to the ambient atmosphere and the
58 potential influence of the synergy of NO_2 and O_2 on the oxidation rate are very limited (Turšič et al., 2001; He et
59 al., 2014), except a few studies investigated SO_2 oxidation in the presence of NO_2 as well as O_2 (Littlejohn et al.,
60 1993; Shen and Rochelle, 1998; Santachiara et al., 1990). Moreover, previous studies have mainly focused on the
61 reaction in bulk solution and only few studies have investigated the oxidation of SO_2 by NO_2 on aerosol particles
62 (Santachiara et al., 1990, 1993). On aerosol particles, water activity, pH, ionic strength, the presence of other

63 compounds or ions, and the role of particle surface are different from in dilute bulk solution and may affect the
64 reaction process and reaction rate. Therefore, further studies of the multiphase reaction of SO₂ with O₂/NO₂
65 mixtures on aerosol particles are required to determine the kinetic parameters and the mechanism of the reaction.

66 In this study, we investigated the multiphase reaction of SO₂ with O₂ in the presence of NO₂ on CaCO₃
67 particles. We quantified the reactive uptake coefficient of SO₂ due to the reaction with an O₂/NO₂/H₂O mixture.
68 Based on our observations and the existing literature, we further discussed the reaction mechanism. Furthermore,
69 we estimated the role of the multiphase oxidation of SO₂ by O₂ in the presence of NO₂ in the atmosphere.

70 2 Experimental

71 The experiments were conducted using a flow reaction system and the setup is shown in Fig. S1. The
72 experimental setup and procedure used have been described in detail in previous studies (Zhao et al., 2017; Zhao
73 et al., 2011; Liu et al., 2008). A gas mixture of NO₂, SO₂, O₂, N₂, and water vapor reacted with particles
74 deposited on a substrate in the flow reaction cell. The concentrations of SO₂ and NO₂ were controlled using mass
75 flow controllers by varying the flow rates of SO₂ (2,000 ppm in high purity N₂, National Institute of Metrology
76 P.R. China), NO₂ (1,000 ppm in high purity N₂, Messer, Germany), and synthetic air [20% O₂ (high purity grade:
77 99.999%, Beijing Haikeyuanchang Practical Gas Co., Ltd.) and 80% N₂ (high purity grade: 99.999%, Beijing
78 Haikeyuanchang Practical Gas Co., Ltd.)]. Relative humidity (RH) was controlled by regulating the flow rates of
79 reactant gases, dry synthetic air, and humidified synthetic air. Humidified synthetic air was prepared by bubbling
80 synthetic air through fritted glass in water. In some experiments, the O₂ concentrations were varied by regulating
81 the mixing ratios of O₂ and N₂ to investigate the effect of O₂. SO₂/O₂/NO₂/H₂O mixtures flew through the
82 reaction cell and reacted with individual stationary CaCO₃ particles, which were deposited on a Teflon-FEP film
83 substrate annealed to a silicon wafer. RH and temperature were measured using a hygrometer (HMT100, Vaisala,
84 Vantaa, Finland) at the exit of the reaction cell. Additionally, temperature was measured using another small
85 temperature sensor (Pt 100, 1/3 DIN B, Heraeus, Hanau, Germany) in the reaction cell. All the experiments were
86 conducted at 298 ± 0.5 K. The experiments were conducted under two RHs (72% and 82%) at 75 ppm SO₂ and
87 75 ppm NO₂.

88 During the reaction, particles were monitored *in-situ* via a glass window on the top of the reaction cell using
89 a Micro-Raman spectrometer (LabRam HR800, HORIBA Jobin Yvon, Kyoto, Japan) to obtain microscopic
90 images and Raman spectra. A 514-nm excitation laser was used, and back scattering Raman signals were detected.
91 The details of the instrument are described elsewhere (Liu et al., 2008; Zhao et al., 2011). Because the particles
92 were larger than the laser spot in this study (~1.5 μm), confocal Raman mapping was used to measure the spectra
93 at different locations on a particle to obtain the chemical information of the entire particle. The mapping area was
94 rectangular and was slightly larger than the particle, with mapping steps of 1 × 1 μm. Raman spectra in the range
95 of 800–3,900 cm⁻¹ were acquired with an exposure time of 1 s for each mapping point. Raman spectra were
96 analyzed using LabSpec 5 software (HORIBA Jobin Yvon). Raman peaks were fitted to Gaussian–Lorentzian
97 functions to obtain peak positions and peak areas at different locations on the particle. The peak areas were then
98 added together to obtain the peak area for the entire particle.

99 Particles of CaCO_3 (98%, Sigma-Aldrich, USA), with average diameters of about 7–10 μm as specified by
100 the supplier, were used in the experiments. The CaCO_3 particles were rhombohedron crystals; X-ray diffraction
101 analysis indicated that they were calcite (Fig. S2). Individual particles were prepared by dripping a dilute CaCO_3
102 suspended solution onto Teflon-FEP film using a pipette and then drying the sample in an oven at 80°C for 10 h.

103 The amount of CaSO_4 as a reaction product was quantified based on Raman peak areas and particle sizes.
104 The details of the method are described in our previous study (Zhao et al., 2017). Briefly, the amount of reaction
105 product CaSO_4 formed was determined as a function of time using Raman peak areas. Raman peak areas were
106 converted to the amount of compound formed using a calibration curve obtained from pure CaSO_4 particles of
107 different sizes, which were determined according to microscopic images. The reaction rate, i.e., the sulfate
108 production rate, was derived from the amount of sulfate formed as a function of time. The reactive uptake
109 coefficient of SO_2 for sulfate formation (γ) was further determined from the reaction rate and collision rate of SO_2
110 on the surface of a single particle.

$$111 \quad \gamma = \frac{\frac{d\{\text{SO}_4^{2-}\}}{dt}}{Z} \quad (1)$$

$$112 \quad Z = \frac{1}{4}cA_s[\text{SO}_2], \quad (2)$$

$$113 \quad c = \sqrt{\frac{8RT}{\pi M_{\text{SO}_2}}} \quad , \quad (3)$$

114 where R is the gas constant, T is temperature, M_{SO_2} is the molecular weight of SO_2 , c is the mean molecular
115 velocity of SO_2 , A_s is the surface area of an individual particle, and Z is the collision rate of SO_2 on the surface of
116 a particle. $\{\text{SO}_4^{2-}\}$ indicates the amount of sulfate in the particle phase in moles. The average reaction rate and
117 surface area of particles during the multiphase reaction period were used to derive the reactive uptake coefficient.
118 The period was chosen to start after the induction period when ~10% of the final sulfate was formed. $[\text{SO}_2]$
119 indicates the concentration of SO_2 in the gas phase.

120 The influence of gas phase diffusion on reactive uptake was evaluated using the resistor model described by
121 Davidovits et al. (2006) and references therein, as well as using the gas phase diffusion correction factor for a
122 reactive uptake coefficient according to the method described by Pöschl et al. (2007). The reactive uptake of SO_2
123 was found to not be limited by gas phase diffusion (see details in the Supplement S1).

124 In addition, we conducted experiments of the reaction SO_2 with only O_2 on both CaCO_3 solid particles and
125 internally mixed $\text{CaCO}_3/\text{Ca}(\text{NO}_3)_2$ particles (with CaCO_3 embedded in $\text{Ca}(\text{NO}_3)_2$ droplets), while keeping other
126 conditions the same as the reaction of SO_2 with an O_2/NO_2 mixture. These experiments of the multiphase
127 oxidation of SO_2 by O_2 can help determine the role of NO_2 in the reaction of SO_2 with an O_2/NO_2 mixture.

128 3 Results and discussion

129 3.1 Reaction products and changes in particle morphology

130 Figure 1 shows the Raman spectra of a CaCO_3 particle during the multiphase reaction of SO_2 with $\text{O}_2/\text{NO}_2/\text{H}_2\text{O}$
131 on its surface. The peak at $1,087 \text{ cm}^{-1}$ was assigned to the symmetric stretching of carbonate ($v_s(\text{CO}_3^{2-})$)
132 (Nakamoto, 1997). During the reaction, the peak at $1,087 \text{ cm}^{-1}$ decreased continuously and finally disappeared as
133 new peaks were observed. The peak at $1,050 \text{ cm}^{-1}$ was assigned to the symmetric stretching of nitrate ($v_s(\text{NO}_3^-)$).

134 The peaks at 1,010 cm⁻¹ and 1,136 cm⁻¹ were assigned to the symmetric stretching ($\nu_s(\text{SO}_4^{2-})$) and asymmetric
135 stretching($\nu_{as}(\text{SO}_4^{2-})$) of sulfate in gypsum ($\text{CaSO}_4 \cdot 2\text{H}_2\text{O}$), respectively (Sarma et al., 1998). In addition, after the
136 reaction, a broad envelope in the range of 2,800–3,800 cm⁻¹ assigned to the stretching of the OH bond in water
137 molecules was observed. Above this envelope, there were two peaks at 3,408 cm⁻¹ and 3,497 cm⁻¹, which were
138 assigned to OH bond stretching in crystallization water of $\text{CaSO}_4 \cdot 2\text{H}_2\text{O}$ (Sarma et al., 1998; Ma et al., 2013).

139 During the multiphase reaction with the $\text{SO}_2/\text{O}_2/\text{NO}_2/\text{H}_2\text{O}$ mixture, the CaCO_3 particles displayed a remarkable
140 change in morphology. The original CaCO_3 particle was a rhombohedron crystal (Fig. 2, panel i, a). As the
141 reaction proceeded, its edges became smoother and later a transparent droplet layer formed, which had a newly
142 formed solid phase embed in it (Fig. 2, panel i, d). The size of the new solid phase grew during the reaction (Fig.
143 2, panel i, d–f) and it seemed to contain many micro-crystals. Raman mapping revealed that the new solid phase
144 consisted of $\text{CaSO}_4 \cdot 2\text{H}_2\text{O}$ (Fig. 2, panel iv), and the surrounding aqueous layer consisted of $\text{Ca}(\text{NO}_3)_2$ (Fig. 2,
145 panel iii).

146 The particle morphology change shown in Fig. 2 was significantly different from the morphology change in
147 the direct reaction of SO_2 with NO_2 (Zhao et al., 2017), where the CaCO_3 particle was first converted to a
148 spherical $\text{Ca}(\text{NO}_3)_2$ droplet and then needle-shaped CaSO_4 crystals formed inside the droplet (Zhao et al., 2017).
149 Moreover, the amount of CaSO_4 formed in this study was much higher than that in the direct reaction of SO_2 with
150 NO_2 . The CaSO_4 solid particle constituted a significant fraction of the volume of the droplet, while in the direct
151 reaction of SO_2 with NO_2 the few needle-shaped CaSO_4 crystals that formed only constituted a small fraction of
152 the droplet volume (Zhao et al., 2017).

153 3.2 Reaction process

154 During the reaction, the amounts of carbonate, nitrate, and sulfate were determined as a function of time, as
155 shown in Fig. 3. At the beginning of the reaction, the amount of carbonate decreased slowly, while the amount of
156 nitrate and sulfate increased slowly. After a period of induction of around 50 min, the reaction accelerated
157 significantly, leading to a rapid consumption of carbonate and production of nitrate and sulfate. The decrease in
158 the amount of carbonate and the increase in the amount of nitrate was because carbonate reacted continuously
159 with NO_2 and H_2O , forming $\text{Ca}(\text{NO}_3)_2$. The detailed mechanism of the multiphase reaction of carbonate with NO_2
160 and H_2O were discussed in our previous studies (Li et al., 2010; Zhao et al., 2017). The mechanism of sulfate
161 formation is discussed in detail in Section 3.4 of the present study. Finally, the carbonate was completely
162 consumed, and the amounts of nitrate and sulfate levelled off.

163 Figure 3 shows that nitrate and sulfate were formed simultaneously during the reaction. This contrasts with
164 the observations made during the direct reaction of SO_2 with NO_2 , where nitrate was formed first, and sulfate was
165 essentially formed after the complete conversion of CaCO_3 particles to $\text{Ca}(\text{NO}_3)_2$ droplets (Zhao et al., 2017).
166 Moreover, the time taken for carbonate to be completely consumed was longer in this study than in the direct
167 reaction of SO_2 with NO_2 (~120 vs. ~40 min) when other conditions were kept the same (Zhao et al., 2017).

168 3.3 Reactive uptake coefficient of SO_2

169 The reactive uptake coefficients of SO_2 for sulfate formation (γ) in the reaction of SO_2 with the
170 $\text{O}_2/\text{NO}_2/\text{H}_2\text{O}/\text{N}_2$ mixture on CaCO_3 with various O_2 concentrations are shown in Table 1. The value of γ for the

171 reaction of SO_2 with O_2/NO_2 at three O_2 concentrations (5, 20, and 86%) was in the range of $(0.35\text{--}1.7) \times 10^{-5}$,
172 and was 1.2×10^{-5} in synthetic air. This latter value was 2–3 orders of magnitude higher than that for the reaction
173 of SO_2 directly with NO_2 under similar conditions (Zhao et al., 2017). When other conditions were kept constant,
174 γ increased with the O_2 concentration. This indicates that O_2 played a key role in enhancing the oxidation rate of
175 SO_2 .

176 The role of O_2 in enhancing the reactive uptake of SO_2 reported here is consistent with the findings in some
177 previous studies. For example, Littlejohn et al. (1993)'s data showed that sulfite oxidation rate increases with the
178 O_2 concentration (0–5% by volume). Shen and Rochelle (1998) also found that in the presence of O_2 , the aqueous
179 sulfite oxidation rate is enhanced. By investigating the oxidation of SO_2 by NO_2 in monodispersed water droplets
180 growing on carbon nuclei, Santachiara et al. (1990) found that sulfate formation rate with 2% O_2 is much higher
181 than that without O_2 . Yet, our findings, as well as those in the studies referred to above, are in contrast to those
182 reported by Lee and Schwartz (1983), who found that changing from N_2 to air as a carrier gas only increases
183 bisulfite oxidation rate by no more than 10%. The difference between our study and Lee and Schwartz (1983)
184 could be due to the difference in O_2 diffusion from gas to the condensed phase and the different mechanisms
185 between the multiphase reaction on particles and the aqueous reaction.

186 Only few studies have reported the S(IV) oxidation rate in the reaction of S(IV) with O_2/NO_2 mixtures
187 (Turšič et al., 2001; Littlejohn et al., 1993). However, due to the limiting step by the aqueous phase mass transfer,
188 it is difficult to quantitatively compare the reaction rates in those studies with the uptake coefficient in our study
189 and the rate constants determined by Lee and Schwartz (1983) and Clifton et al. (1988). For example, a rate
190 constant of $2.4 \times 10^3 \text{ mol}^{-1} \text{ L s}^{-1}$ (at pH 3) can be derived from the results of Turšič et al. (2001), which is much
191 lower than the values reported by Lee and Schwartz (1983) and Clifton et al. (1988). This can be attributed to the
192 limiting step by the aqueous-phase mass transfer because the characteristic mixing time in the aqueous phase in
193 Turšič et al. (2001) was likely much longer than that of Lee and Schwartz (1983) (1.7–5.3 s), according to the
194 HSO_3^- concentration time series reported by Turšič et al. (2001).

195 3.4 Reaction mechanism

196 In the multiphase reaction of SO_2 with $\text{O}_2/\text{NO}_2/\text{H}_2\text{O}$ on CaCO_3 particles, we found that CaCO_3 reacted with
197 NO_2 and H_2O and produced $\text{Ca}(\text{NO}_3)_2$, which deliquesced, forming liquid water, and provided a site for the
198 aqueous oxidation of SO_2 . This process is similar to the direct reaction of SO_2 with NO_2 on CaCO_3 particles. The
199 details of this part of the reaction mechanism were discussed in our previous study (Zhao et al., 2017).

200 Once the aqueous phase was formed, SO_2 could undergo multiphase reactions with O_2/NO_2 . The mechanism
201 of the direct aqueous reaction of S(IV) with NO_2 in the absence of O_2 is complex. Previous studies have proposed
202 two different mechanisms for the reaction. One involves SO_3^- radical formation (Littlejohn et al., 1993; Shen and
203 Rochelle, 1998; Turšič et al., 2001), while the other involves the formation of $\text{NO}_2\text{--S(IV)}$ complexes (Clifton et
204 al., 1988), but no radical formation.

205 According to the $\text{NO}_2\text{--S(IV)}$ adduct mechanism, the presence of O_2 should not affect the SO_2 oxidation rate;
206 however, in this study, a substantial enhancement in the SO_2 oxidation rate was observed in the presence of O_2
207 compared with that in the absence of O_2 . Therefore, the $\text{NO}_2\text{--S(IV)}$ adduct mechanism was not considered to
208 have been important in this study.

209 In the free-radical mechanism, the $\text{SO}_3^{\cdot-}$ radical is proposed to be formed (R7, Table 2), which is based on
210 the observation of $\text{S}_2\text{O}_6^{2-}$ formation, with $\text{S}_2\text{O}_6^{2-}$ known to be the combination reaction product of $\text{SO}_3^{\cdot-}$ (Eriksen,
211 1974; Hayon et al., 1972; Deister and Warneck, 1990; Brandt et al., 1994; Waygood and McElroy, 1992). In
212 addition to SO_4^{2-} and NO_2^- , $\text{S}_2\text{O}_6^{2-}$ was detected with an appreciable yield using Raman spectroscopy, following
213 the reaction of NO_2 with aqueous sulfite (Littlejohn et al., 1993). $\text{S}_2\text{O}_6^{2-}$ was also observed in the aqueous
214 oxidation of bisulfite in an N_2 -saturated solution in the presence of Fe(III) using ion-interaction chromatography
215 (Podkrajšek et al., 2002). The $\text{SO}_3^{\cdot-}$ radical can react via two pathways, forming either $\text{S}_2\text{O}_6^{2-}$ or SO_4^{2-} (R8–R10,
216 Table 2). The reactions R8–R10 have been well established in studies of S(IV) oxidation by other pathways,
217 including OH oxidation, photo-oxidation, and transition metal catalyzed oxidation (Eriksen, 1974; Hayon et al.,
218 1972; Deister and Warneck, 1990; Brandt et al., 1994; Brandt and Vaneldik, 1995; Waygood and McElroy, 1992).
219 In addition, although previous studies have not reported the direct observation of the $\text{SO}_3^{\cdot-}$ radical in the aqueous
220 reaction of S(IV) with NO_2 , $\text{SO}_3^{\cdot-}$ was observed in the reaction of NO_2^- with SO_3^{2-} in an acidic buffer solution
221 ($\text{pH} = 4.0$) using electron spin resonance (ESR) (Shi, 1994). Because NO_2^- is formed in the aqueous reaction of
222 SO_2 with NO_2 , and $\text{S}_2\text{O}_6^{2-}$ as the combination reaction product of $\text{SO}_3^{\cdot-}$ is observed (Littlejohn et al., 1993), $\text{SO}_3^{\cdot-}$
223 formation is plausible.

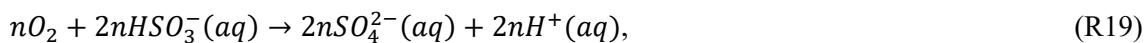
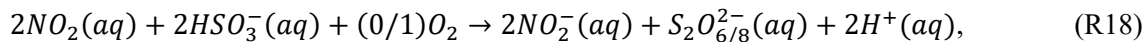
224 In the presence of O_2 , the $\text{SO}_3^{\cdot-}$ radical can react rapidly with O_2 , forming the $\text{SO}_5^{\cdot-}$ radical (R11, Table 2).
225 Following this reaction, a number of chain reactions can occur to ultimately form sulfate (Littlejohn et al., 1993;
226 Seinfeld and Pandis, 2006; Shen and Rochelle, 1998) (R12–R15, Table 2). Littlejohn et al. (1993) observed that
227 the amount of $\text{S}_2\text{O}_6^{2-}$ relative to SO_4^{2-} formed in the aqueous reaction of NO_2 with sulfite decreases in the
228 presence of O_2 compared with the reaction in the absence of O_2 . At low NO_2 concentrations (< 5 ppm), $\text{S}_2\text{O}_6^{2-}$ is
229 undetectable in the presence of O_2 . This indicates that O_2 suppresses the reaction pathway of $\text{S}_2\text{O}_6^{2-}$ formation
230 (R8, Table 2). Because the $\text{SO}_3^{\cdot-}$ radical can react rapidly with O_2 , forming the $\text{SO}_5^{\cdot-}$ radical, and would therefore
231 be consumed, the suppression of $\text{S}_2\text{O}_6^{2-}$ formation can be attributed to the reaction of $\text{SO}_3^{\cdot-}$ with O_2 (R11, Table
232 2). The reactions R11–R15 have been well established by studies of the oxidation of S(IV) by OH or
233 photo-oxidation, and all the radicals have been observed (Hayon et al., 1972; Huie et al., 1989; Huie and Neta,
234 1987; Chameides and Davis, 1982; Seinfeld and Pandis, 2006).

235 The free-radical chain mechanism is consistent with the findings of this study and is therefore more plausible.
236 The enhancement of the SO_2 oxidation rate in the reaction of SO_2 with $\text{O}_2/\text{NO}_2/\text{H}_2\text{O}$ on CaCO_3 particles
237 compared with that in the direct reaction of SO_2 with $\text{NO}_2/\text{H}_2\text{O}$ was attributed to O_2 . Although during the reaction
238 in the absence of O_2 —i.e., the direct oxidation of SO_2 by NO_2 —the $\text{SO}_3^{\cdot-}$ radical can be formed (R7), the reaction
239 chain cannot propagate (R11–R15). Therefore, the S(IV) oxidation rate and the reactive uptake coefficient of SO_2
240 were much lower than that in the presence of O_2 . According to the difference between the reactive uptake
241 coefficient in this study and in the direct reaction of SO_2 with NO_2 (Zhao et al., 2017), the sulfate production rate
242 via chain reactions due to the presence of O_2 (20%) was 2–3 orders of magnitude faster than the direct oxidation
243 of SO_2 by NO_2 . This indicates that sulfate production in the reaction of SO_2 with O_2/NO_2 was largely due to O_2
244 oxidation via the chain reaction pathway, i.e., “autoxidation” of S(IV), rather than the direct oxidation of SO_2 by
245 NO_2 and thus O_2 was the main oxidant of SO_2 .

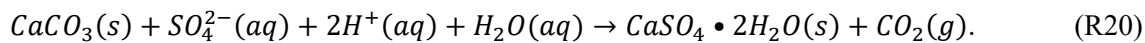
246 Although the direct oxidation of SO_2 by NO_2 only accounted for a very small fraction of sulfate formation,
247 NO_2 played an important role in the SO_2 oxidation by initiating the chain reactions via the production of the $\text{SO}_3^{\cdot-}$

radical (R7). In the experiment without NO_2 , but with other reaction conditions the same, we were unable to detect sulfate after 5 h of reaction. This indicates that O_2 by itself cannot initiate the chain reactions (although it favors chain propagation), and that the oxidation of SO_2 by O_2 was slow. The effect on the SO_2 oxidation rate when both NO_2 and O_2 were present was much higher than the sum of the effect of NO_2 and O_2 . We refer to this effect as the synergy of NO_2 and O_2 , which resulted in the fast oxidation of SO_2 to form sulfate in this study. This effect is similar to a “ternary” reaction found with the reaction of NO_2 –particles– H_2O or SO_2 –particles– O_3 (Zhu et al., 2011), where the reaction rate can be much faster than the sum of the reaction rates for the reaction of the second and third reactant with the first reactant. In addition to acting as the initiator of chain reactions, NO_2 also contributed to the formation of the aqueous phase through the reaction with CaCO_3 , forming $\text{Ca}(\text{NO}_3)_2$ as discussed above, which provided a site for S(IV) oxidation.

Based on the discussion above, we summarize the reaction mechanism that occurred in this study in Table 2. The reactions are classified as chain initiation, chain propagation, and chain termination. The dominant S(IV) species depends on pH. Due to the fast dissociations of $\text{SO}_2\bullet\text{H}_2\text{O}$ and HSO_3^- , reactions consuming one of these S(IV) species will result in instantaneous re-establishment of the equilibria between them (Seinfeld and Pandis, 2006). In this study, the pH of the aqueous layer of $\text{Ca}(\text{NO}_3)_2$ may change dynamically with time during the reaction and may not be completely homogeneous within the aqueous droplet. The pH values could vary between ~ 3 and ~ 7.6 . In the surface of the aqueous layer, pH was mainly determined by the gas–aqueous equilibrium of SO_2 , and was estimated to be ~ 3 . In the vicinity of the CaCO_3 core, pH was mainly determined by the hydrolysis of carbonate and was estimated to be ~ 7.6 . It is likely that both HSO_3^- and SO_3^{2-} were present, and the dominant species depended on the reaction time and location within the aqueous droplet. Nevertheless, to make the reaction mechanism clearer, HSO_3^- was used in the reaction equations. Similar reaction equations are also applicable to SO_3^{2-} because of the fast dissociations of $\text{SO}_2\bullet\text{H}_2\text{O}$ and HSO_3^- . Overall, the reaction can be written as follows, which clearly shows that O_2 was the main oxidant for sulfate formation:



where $n \gg 1$. Once sulfuric acid was formed, it reacted with CaCO_3 , forming CaSO_4 :



As mentioned above, compared with the direct reaction of SO_2 with NO_2 , CaCO_3 was consumed more slowly in the reaction with O_2/NO_2 . There were two possible reasons for this. First, the $\text{CaSO}_4 \bullet 2\text{H}_2\text{O}$ formed in the reaction could cover the CaCO_3 surface and partly suppress the diffusion of aqueous ions, such as protons, and also limit the contact of reactants with the surface of the CaCO_3 particles, thus reducing the CaCO_3 consumption rate. Second, compared with the direct reaction of SO_2 with NO_2 , a much higher fraction of CaCO_3 was converted to $\text{CaSO}_4 \bullet 2\text{H}_2\text{O}$ instead of $\text{Ca}(\text{NO}_3)_2$ due to the fast production of $\text{CaSO}_4 \bullet 2\text{H}_2\text{O}$. Therefore, the volume of a $\text{Ca}(\text{NO}_3)_2$ droplet was much smaller than that in the direct reaction of SO_2 with NO_2 for a given CaCO_3 particle. Because the uptake rate of NO_2 was proportional to the droplet surface area and the NO_2 hydrolysis rate was proportional to the droplet volume, the rate of nitric acid production from NO_2 hydrolysis and its reaction rate with CaCO_3 were reduced. Therefore, the CaCO_3 particles were consumed more slowly in the reaction with O_2/NO_2 .

286 4 Conclusion and implications

287 We investigated the multiphase reaction of SO_2 with $\text{O}_2/\text{NO}_2/\text{H}_2\text{O}$ on CaCO_3 particles. The reaction
288 converted CaCO_3 particles to $\text{Ca}(\text{NO}_3)_2$ droplets, in which $\text{CaSO}_4 \cdot 2\text{H}_2\text{O}$ was embedded and accounted for a
289 significant fraction of the droplet volume by the end of the reaction. The $\text{Ca}(\text{NO}_3)_2$ droplet formed by the reaction
290 of CaCO_3 with NO_2 provided a site for the multiphase oxidation of SO_2 . Generally, nitrate and sulfate were
291 formed simultaneously. The reactive uptake coefficient of SO_2 for sulfate formation in the reaction of SO_2 with
292 $\text{NO}_2/\text{H}_2\text{O}$ in synthetic air was determined to be around 10^{-5} . Compared with the reaction of SO_2 with NO_2 on a
293 CaCO_3 particle in the absence of O_2 , i.e., the direct oxidation of SO_2 by NO_2 in N_2 , sulfate production rate in the
294 reaction of SO_2 with O_2/NO_2 was enhanced by 2–3 orders of magnitude. According to the findings of this study
295 and the existing literature, SO_2 oxidation likely proceeded via a free-radical chain reaction mechanism. O_2 was
296 the main oxidant of SO_2 , and NO_2 mainly acted as an initiator of the chain reactions. The synergy of NO_2 and O_2
297 resulted in the fast oxidation of SO_2 . The absence of either NO_2 or O_2 led to much slower SO_2 oxidation.

298 Using a method developed in our previous study (Zhao et al., 2017), we assessed the importance of the
299 multiphase oxidation of SO_2 by O_2 in the presence of NO_2 by estimating the lifetime of SO_2 due to multiphase
300 reactions and the lifetime due to the gas phase reaction (with the OH radical). The lifetime of SO_2 due to the
301 multiphase reaction of SO_2 with O_2/NO_2 was estimated to be around 20 days using the reactive uptake coefficient
302 of SO_2 (1.2×10^{-5}) and the typical particle surface area concentration for mineral aerosols in winter in Beijing
303 ($6.3 \times 10^{-6} \text{ cm}^2 \text{ cm}^{-3}$) (Huang et al., 2015). This lifetime is comparable to the lifetime of SO_2 due to the gas phase
304 reaction with OH , which is ~ 12 days assuming that the daytime OH concentration is $1 \times 10^6 \text{ molecules cm}^{-3}$
305 (Lelieveld et al., 2016; Prinn et al., 2005). Therefore, we conclude that the multiphase oxidation of SO_2 by O_2 in
306 the presence of NO_2 is likely to be an important source of sulfate and a sink of SO_2 in the ambient atmosphere,
307 and can play a significant role in the sulfate formation during severe haze episodes, such as those that frequently
308 occur in China. During haze episodes, there are high concentrations of SO_2 and NO_2 and relative humidity is
309 often high (Zhang et al., 2014; Wang et al., 2016; Zheng et al., 2015b). Under these conditions, the multiphase
310 oxidation of SO_2 by O_2 in the presence of NO_2 could proceed rapidly, forming sulfate. The enhanced sulfate
311 concentration due to multiphase reactions and resulting aerosol water content can further promote the multiphase
312 oxidation of SO_2 . The reaction thus proceeds in a self-accelerating way. Therefore, it can contribute significantly
313 to sulfate formation during haze episodes, which could explain the discrepancies between the observed and
314 modelled sulfate concentrations (Cheng et al., 2016; Gao et al., 2016; Wang et al., 2016; Zheng et al., 2015a).

315 In addition, elucidating the mechanism of the multiphase reaction of SO_2 with $\text{O}_2/\text{NO}_2/\text{H}_2\text{O}$ in the
316 atmosphere is important for the other atmospheric implications of the reaction besides sulfate formation.
317 According to the reaction mechanism, the direct oxidation of SO_2 by NO_2 forms sulfate and nitrite, with a
318 stoichiometry of 1:1, and nitrite can further form HONO under acidic conditions. The HONO could then
319 evaporate into the atmosphere, where it would be an important source of OH radical. If NO_2 were the main
320 oxidant of SO_2 in the multiphase reaction, the reaction would form one HONO molecule for every sulfate formed.
321 Thus, the oxidation of SO_2 by NO_2 can simultaneously be an important source of HONO and OH radical, and
322 SO_2 oxidation would be strongly coupled with reactive nitrogen chemistry. However, according to the
323 mechanism of this study, NO_2 only acted as an initiator of the chain reactions in SO_2 oxidation and essentially all
324 the SO_2 was oxidized by O_2 . Therefore, the amount of HONO formation per sulfate formed was trivial. The

325 oxidation of SO_2 by O_2/NO_2 is expected to be neither an important source of HONO and OH in the atmosphere
326 nor to have a significant influence on reactive nitrogen chemistry.

327

328 **Acknowledgements**

329 This work was supported by Natural Science Foundation Committee of China (41421064, 21190051,
330 40490265, 91544000) and Ministry of Science and Technology (Grant No. 2002CB410802).

331 **References**

332 Brandt, C., Fabian, I., and Vaneldik, R.: Kinetics and mechanism of the iron(III)-catalyzed autoxidation of
333 sulfur(IV) oxides in aqueous-solution - evidence for the redox cycling of iron in the presence of oxygen and
334 modeling of the overall reaction-mechanism, *Inorg. Chem.* , 33, 687-701, 10.1021/ic00082a012, 1994.

335 Brandt, C., and Vaneldik, R.: Transition metal-catalyzed oxidation of sulfur (IV) oxides. Atmospheric-relevant
336 processes and mechanisms, *Chem. Rev.*, 95, 119-190, 10.1021/cr00033a006, 1995.

337 Chameides, W. L., and Davis, D. D.: The free-radical chemistry of cloud droplets and its impact upon the
338 composition of rain, *J. Geophys. Res.-Oceans*, 87, 4863-4877, 10.1029/JC087iC07p04863, 1982.

339 Cheng, Y. F., Zheng, G. J., Wei, C., Mu, Q., Zheng, B., Wang, Z. B., Gao, M., Zhang, Q., He, K. B., Carmichael,
340 G., Poschl, U., and Su, H.: Reactive nitrogen chemistry in aerosol water as a source of sulfate during haze events
341 in China, *Sci. Adv.*, 2, 10.1126/sciadv.1601530, 2016.

342 Clifton, C. L., Altstein, N., and Huie, R. E.: Rate-constant for the reaction of NO₂ with sulfur(IV) over the pH
343 range 5.3-13, *Environ. Sci. Technol.*, 22, 586-589, 10.1021/es00170a018, 1988.

344 Davidovits, P., Kolb, C. E., Williams, L. R., Jayne, J. T., and Worsnop, D. R.: Mass accommodation and
345 chemical reactions at gas-liquid interfaces, *Chem. Rev.*, 106, 1323-1354, 10.1021/cr040366k, 2006.

346 Deister, U., and Warneck, P.: Photooxidation of sulfite (SO₃²⁻) in aqueous solution, *J. Phys. Chem.*, 94,
347 2191-2198, 10.1021/j100368a084, 1990.

348 Eriksen, T. E.: pH Effects on the pulse radiolysis of deoxygenated aqueous solutions of sulphur dioxide, *Journal*
349 of the Chemical Society, Faraday Transactions 1: Physical Chemistry in Condensed Phases, 70, 208-215,
350 10.1039/f19747000208, 1974.

351 Gao, M., Carmichael, G. R., Wang, Y., Ji, D., Liu, Z., and Wang, Z.: Improving simulations of sulfate aerosols
352 during winter haze over Northern China: the impacts of heterogeneous oxidation by NO₂, *Front. Environ. Sci.*
353 Eng., 10, 16, 10.1007/s11783-016-0878-2, 2016.

354 Guo, H., Weber, R. J., and Nenes, A.: High levels of ammonia do not raise fine particle pH sufficiently to yield
355 nitrogen oxide-dominated sulfate production, *Sci. Rep.*, 7, 12109, 10.1038/s41598-017-11704-0, 2017.

356 Hayon, E., Treinin, A., and Wilf, J.: Electronic spectra, photochemistry, and autoxidation mechanism of the
357 sulfite-bisulfite-pyrosulfite systems. SO₂⁻, SO₃⁻, SO₄⁻, and SO₅⁻ radicals, *J. Am. Chem. Soc.* , 94, 47-57,
358 10.1021/ja00756a009, 1972.

359 He, H., Wang, Y., Ma, Q., Ma, J., Chu, B., Ji, D., Tang, G., Liu, C., Zhang, H., and Hao, J.: Mineral dust and
360 NO_x promote the conversion of SO₂ to sulfate in heavy pollution days, *Sci. Rep.*, 4, 10.1038/srep04172, 2014.

361 Huang, L., Zhao, Y., Li, H., and Chen, Z.: Kinetics of Heterogeneous Reaction of Sulfur Dioxide on Authentic
362 Mineral Dust: Effects of Relative Humidity and Hydrogen Peroxide, *Environ. Sci. Technol.*, 49, 10797-10805,
363 10.1021/acs.est.5b03930, 2015.

364 Huie, R. E., and Neta, P.: Kinetics of one-electron transfer-reactions involving ClO₂ and NO₂, *J. Phys. Chem.* ,
365 90, 1193-1198, 10.1021/j100278a046, 1986.

366 Huie, R. E., and Neta, P.: Rate constants for some oxidations of S(IV) by radicals in aqueous-solutions, *Atmos.*
367 *Environ.*, 21, 1743-1747, 10.1016/0004-6981(87)90113-2, 1987.

368 Huie, R. E., Clifton, C. L., and Altstein, N.: A pulse radiolysis and flash photolysis study of the radicals SO₂,
369 SO₃, SO₄ and SO₅, *Radiat. Phys. Chem.* , 33, 361-370, 1989.

370 Lee, Y.-N., and Schwartz, S. E.: Kinetics of oxidation of aqueous sulfur (IV) by nitrogen dioxide, in:
371 Precipitation Scavenging, Dry Deposition and Resuspension, edited by: Pruppacher, H. R., Semonin, R. G., and
372 Slinn, W. G. N., Elsevier, New York, 453-466, 1983.

373 Lelieveld, J., Gromov, S., Pozzer, A., and Taraborrelli, D.: Global tropospheric hydroxyl distribution, budget and
374 reactivity, *Atmos. Chem. Phys.*, 16, 12477-12493, 10.5194/acp-16-12477-2016, 2016.

375 Li, H. J., Zhu, T., Zhao, D. F., Zhang, Z. F., and Chen, Z. M.: Kinetics and mechanisms of heterogeneous
376 reaction of NO₂ on CaCO₃ surfaces under dry and wet conditions, *Atmos. Chem. Phys.*, 10, 463-474, 2010.

377 Littlejohn, D., Wang, Y. Z., and Chang, S. G.: Oxidation of aqueous sulfite ion by nitrogen-dioxide, *Environ. Sci.*
378 *Technol.*, 27, 2162-2167, 10.1021/es00047a024, 1993.

379 Liu, M. X., Song, Y., Zhou, T., Xu, Z. Y., Yan, C. Q., Zheng, M., Wu, Z. J., Hu, M., Wu, Y. S., and Zhu, T.: Fine
380 particle pH during severe haze episodes in northern China, *Geophys. Res. Lett.*, 44, 5213-5221,
381 10.1002/2017gl073210, 2017.

382 Liu, Y. J., Zhu, T., Zhao, D. F., and Zhang, Z. F.: Investigation of the hygroscopic properties of Ca(NO₃)₂ and
383 internally mixed Ca(NO₃)₂/CaCO₃ particles by micro-Raman spectrometry, *Atmos. Chem. Phys.*, 8,
384 7205-7215, 2008.

385 Ma, Q., He, H., Liu, Y., Liu, C., and Grassian, V. H.: Heterogeneous and multiphase formation pathways of
386 gypsum in the atmosphere, *Phys. Chem. Chem. Phys.*, 15, 19196-19204, 10.1039/c3cp53424c, 2013.

387 Nakamoto, K.: Infrared and Raman Spectra of Inorganic and Coordination Compounds Part A, John Wiley
388 & Sons, New York, 221-247 pp., 1997.

389 Nash, T.: Effect of nitrogen-dioxide and of some transition-metals on the oxidation of dilute bisulfite solutions,
390 *Atmos. Environ.*, 13, 1149-1154, 10.1016/0004-6981(79)90038-6, 1979.

391 Pöschl, U., Rudich, Y., and Ammann, M.: Kinetic model framework for aerosol and cloud surface chemistry and
392 gas-particle interactions - Part 1: General equations, parameters, and terminology, *Atmos. Chem. Phys.*, 7,
393 5989-6023, 2007.

394 Podkrajšek, B., Grgić, I., and Turšič, J.: Determination of sulfur oxides formed during the S(IV) oxidation in the
395 presence of iron, *Chemosphere*, 49, 271-277, [https://doi.org/10.1016/S0045-6535\(02\)00324-7](https://doi.org/10.1016/S0045-6535(02)00324-7), 2002.

396 Prinn, R. G., Huang, J., Weiss, R. F., Cunnold, D. M., Fraser, P. J., Simmonds, P. G., McCulloch, A., Harth, C.,
397 Reimann, S., Salameh, P., O'Doherty, S., Wang, R. H. J., Porter, L. W., Miller, B. R., and Krummel, P. B.:
398 Evidence for variability of atmospheric hydroxyl radicals over the past quarter century, *Geophys. Res. Lett.*, 32,
399 10.1029/2004gl022228, 2005.

400 Santachiara, G., Prodi, F., and Vivarelli, F.: SO₂ oxidation in monodisperse droplets grown on carbon nuclei in
401 presence of NO₂, *J. Aerosol Sci.*, 21, S221-S224, 10.1016/0021-8502(90)90224-1, 1990.

402 Santachiara, G., Prodi, F., and Vivarelli, F.: Further experiments on SO₂ oxidation rate in monodisperse droplets
403 grown on carbon nuclei in presence of O₂ and NO₂, *J. Aerosol Sci.*, 24, 683-685,
404 10.1016/0021-8502(93)90024-4, 1993.

405 Sarma, L. P., Prasad, P. S. R., and Ravikumar, N.: Raman spectroscopic study of phase transitions in natural
406 gypsum, *J. Raman Spectrosc.*, 29, 851-856, 10.1002/(sici)1097-4555(199809)29:9<851::aid-jrs313>3.0.co;2-s,
407 1998.

408 Seinfeld, J. H., and Pandis, S. N.: Atmospheric chemistry and physics: from air pollution to climate change, 2nd
409 ed., John Wiley & Sons. Inc., 2006.

410 Shen, C. H., and Rochelle, G. T.: Nitrogen Dioxide Absorption and Sulfite Oxidation in Aqueous Sulfite, Environ.
411 Sci. Technol., 32, 1994-2003, 10.1021/es970466q, 1998.

412 Shi, X. L.: Generation of SO_3^- and OH radicals in SO_3^{2-} reactions with inorganic environmental-pollutants and its
413 implications to SO_3^{2-} toxicity, J. Inorg. Biochem. , 56, 155-165, 10.1016/0162-0134(94)85002-x, 1994.

414 Spindler, G., Hesper, J., Bruggemann, E., Dubois, R., Muller, T., and Herrmann, H.: Wet annular denuder
415 measurements of nitrous acid: laboratory study of the artefact reaction of NO_2 with S(IV) in aqueous solution
416 and comparison with field measurements, Atmos. Environ., 37, 2643-2662, 10.1016/s1352-2310(03)00209-7,
417 2003.

418 Turšič, J., Grgić, I., and Bizjak, M.: Influence of NO_2 and dissolved iron on the S(IV) oxidation in synthetic
419 aqueous solution, Atmos. Environ., 35, 97-104, [https://doi.org/10.1016/S1352-2310\(00\)00283-1](https://doi.org/10.1016/S1352-2310(00)00283-1), 2001.

420 Wang, G., Zhang, R., Gomez, M. E., Yang, L., Levy Zamora, M., Hu, M., Lin, Y., Peng, J., Guo, S., Meng, J., Li,
421 J., Cheng, C., Hu, T., Ren, Y., Wang, Y., Gao, J., Cao, J., An, Z., Zhou, W., Li, G., Wang, J., Tian, P.,
422 Marrero-Ortiz, W., Secrest, J., Du, Z., Zheng, J., Shang, D., Zeng, L., Shao, M., Wang, W., Huang, Y., Wang, Y.,
423 Zhu, Y., Li, Y., Hu, J., Pan, B., Cai, L., Cheng, Y., Ji, Y., Zhang, F., Rosenfeld, D., Liss, P. S., Duce, R. A., Kolb,
424 C. E., and Molina, M. J.: Persistent sulfate formation from London Fog to Chinese haze, Proc. Nat. Acad. Sci.
425 U.S.A., 113, 13630-13635, 10.1073/pnas.1616540113, 2016.

426 Waygood, S. J., and McElroy, W. J.: Spectroscopy and decay kinetics of the sulfite radical anion in aqueous
427 solution, J. Chem. Soc.-Faraday Trans., 88, 1525-1530, 10.1039/ft9928801525, 1992.

428 Xue, J., Yuan, Z. B., Griffith, S. M., Yu, X., Lau, A. K. H., and Yu, J. Z.: Sulfate Formation Enhanced by a
429 Cocktail of High NO_x, SO₂, Particulate Matter, and Droplet pH during Haze-Fog Events in Megacities in China:
430 An Observation-Based Modeling Investigation, Environ. Sci. Technol., 50, 7325-7334, 10.1021/acs.est.6b00768,
431 2016.

432 Zhang, J. K., Sun, Y., Liu, Z. R., Ji, D. S., Hu, B., Liu, Q., and Wang, Y. S.: Characterization of submicron
433 aerosols during a month of serious pollution in Beijing, 2013, Atmos. Chem. Phys., 14, 2887-2903,
434 10.5194/acp-14-2887-2014, 2014.

435 Zhao, D., Song, X., Zhu, T., Zhang, Z., and Liu, Y.: Multiphase Reaction of SO₂ with NO₂ on CaCO₃ Particles.
436 1. Oxidation of SO₂ by NO₂, Atmos. Chem. Phys. Discuss., 2017, 1-23, 10.5194/acp-2017-610, 2017.

437 Zhao, D. F., Zhu, T., Chen, Q., Liu, Y. J., and Zhang, Z. F.: Raman micro-spectrometry as a technique for
438 investigating heterogeneous reactions on individual atmospheric particles, Sci. China Chem., 54, 154-160,
439 10.1007/s11426-010-4182-x, 2011.

440 Zheng, B., Zhang, Q., Zhang, Y., He, K. B., Wang, K., Zheng, G. J., Duan, F. K., Ma, Y. L., and Kimoto, T.:
441 Heterogeneous chemistry: a mechanism missing in current models to explain secondary inorganic aerosol
442 formation during the January 2013 haze episode in North China, Atmos. Chem. Phys., 15, 2031-2049,
443 10.5194/acp-15-2031-2015, 2015a.

444 Zheng, G. J., Duan, F. K., Su, H., Ma, Y. L., Cheng, Y., Zheng, B., Zhang, Q., Huang, T., Kimoto, T., Chang, D.,
445 Poschl, U., Cheng, Y. F., and He, K. B.: Exploring the severe winter haze in Beijing: the impact of synoptic

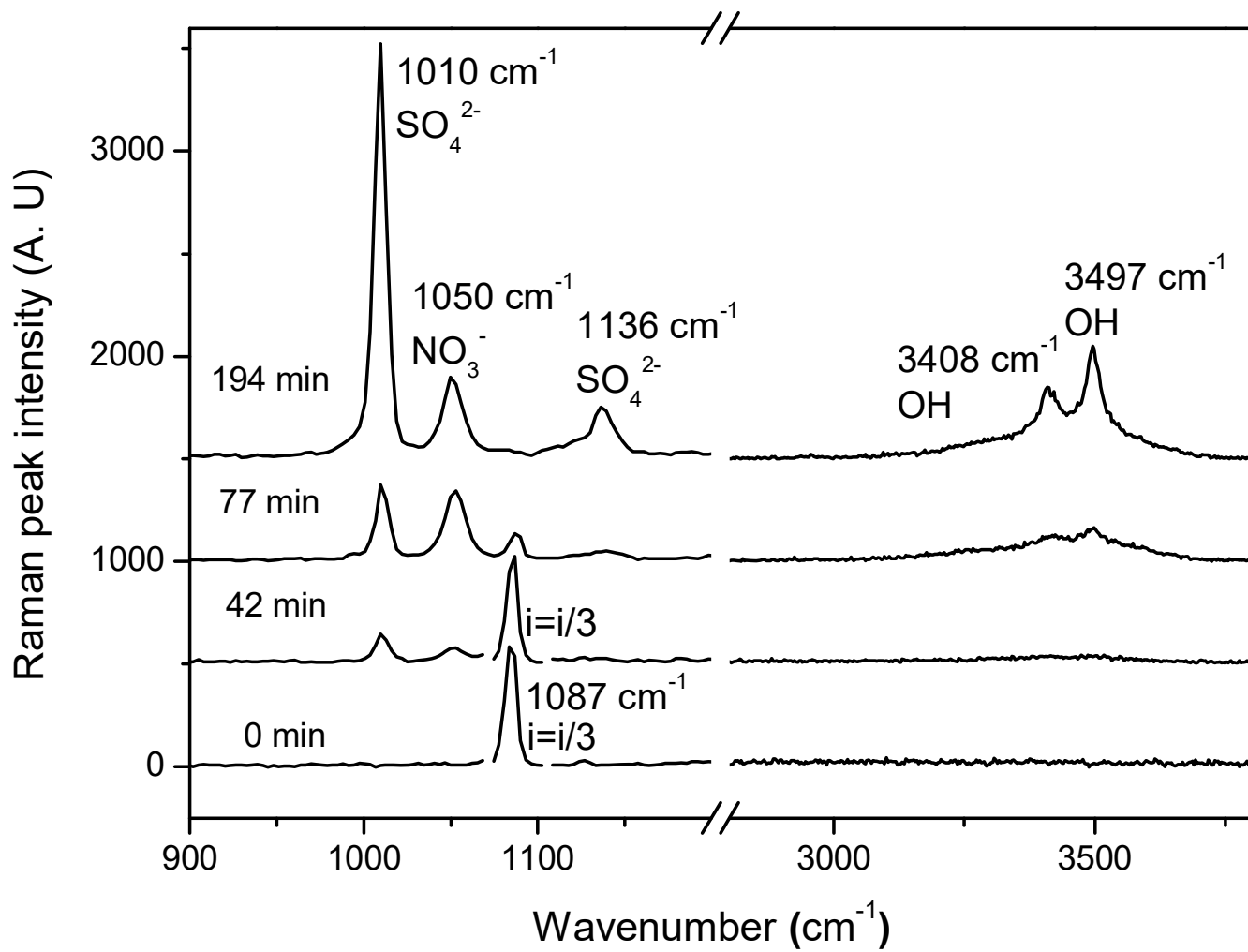
446 weather, regional transport and heterogeneous reactions, *Atmos. Chem. Phys.*, 15, 2969-2983,
447 10.5194/acp-15-2969-2015, 2015b.
448 Zhu, T., Shang, J., and Zhao, D. F.: The roles of heterogeneous chemical processes in the formation of an air
449 pollution complex and gray haze, *Sci. China Chem.*, 54, 145-153, 10.1007/s11426-010-4181-y, 2011.
450
451
452
453

454
455 **Table 1.** Reactive uptake coefficient of SO₂ for sulfate formation at 82% RH and at different O₂
concentrations.

SO₂/NO₂/O₂ concentration	γ
75 ppm/ 75 ppm/ 86 %	1.7×10^{-5}
75 ppm/ 75 ppm/ 20 %	1.2×10^{-5}
75 ppm/ 75 ppm/ 5 %	3.5×10^{-6}

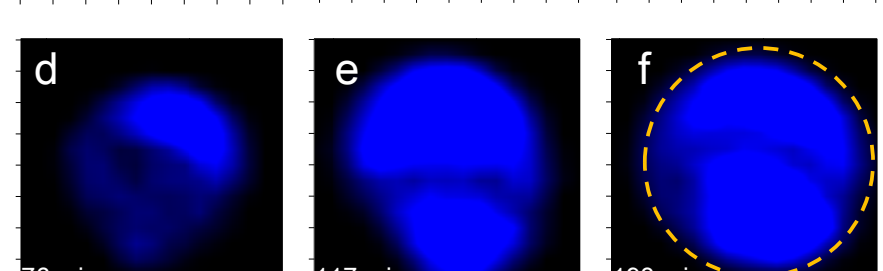
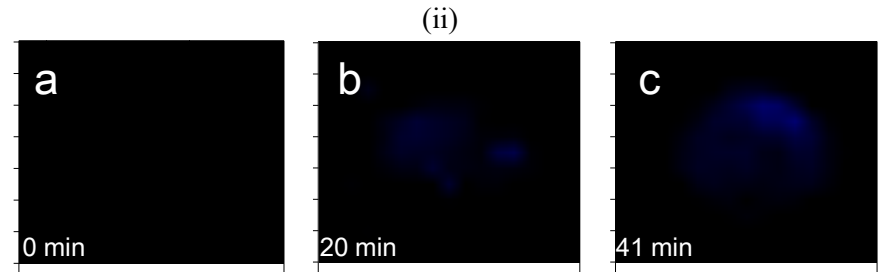
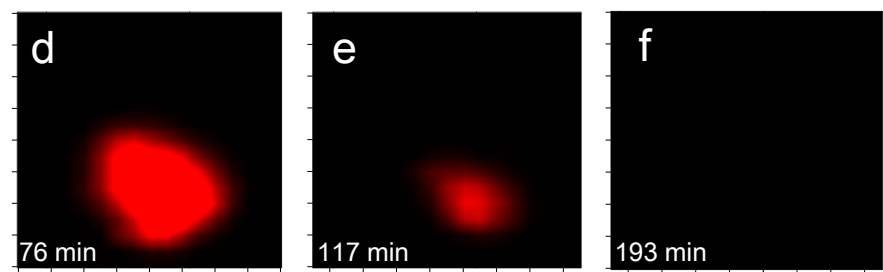
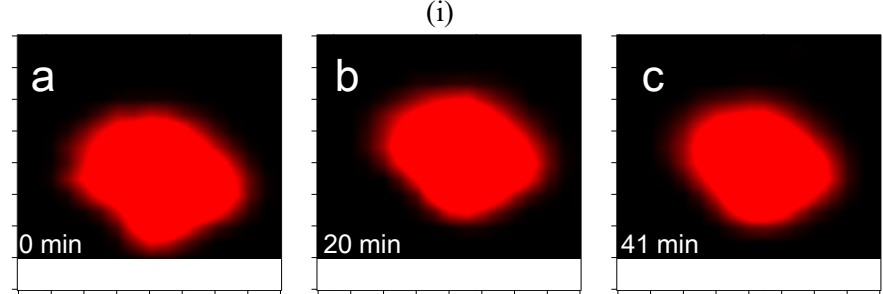
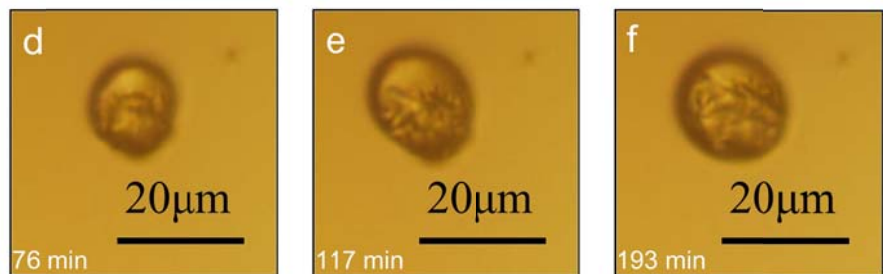
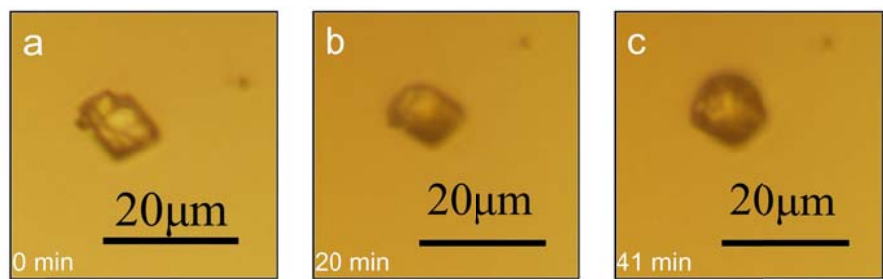
Table 2. Summary of the mechanism of the reaction S(IV) with O₂/NO₂

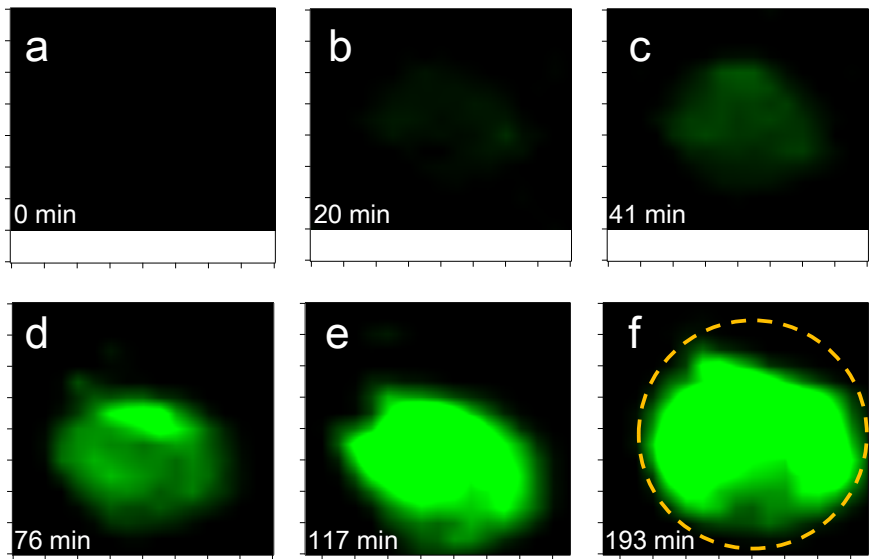
Step	Reactions
Initiation	$\text{NO}_2(\text{aq}) + \text{HSO}_3^-(\text{aq}) \rightarrow \text{NO}_2^-(\text{aq}) + \text{SO}_3^-(\text{aq}) + \text{H}^+(\text{aq})$ (R7)
	$\text{SO}_3^-(\text{aq}) + \text{O}_2(\text{aq}) \rightarrow \text{SO}_5^-(\text{aq})$ (R11)
	$\text{SO}_5^-(\text{aq}) + \text{HSO}_3^-(\text{aq}) \rightarrow \text{HSO}_5^-(\text{aq}) + \text{SO}_3^-(\text{aq})$ (R12)
Propagation	$\text{HSO}_5^-(\text{aq}) + \text{HSO}_3^-(\text{aq}) \rightarrow 2\text{SO}_4^{2-}(\text{aq}) + 2\text{H}^+(\text{aq})$ (R13)
	$\text{SO}_5^-(\text{aq}) + \text{HSO}_3^-(\text{aq}) \rightarrow \text{SO}_4^{2-}(\text{aq}) + \text{SO}_4^-(\text{aq}) + \text{H}^+(\text{aq})$ (R14)
	$\text{SO}_4^-(\text{aq}) + \text{HSO}_3^-(\text{aq}) \rightarrow \text{SO}_4^{2-}(\text{aq}) + \text{SO}_3^-(\text{aq}) + \text{H}^+(\text{aq})$ (R15)
	$\text{SO}_3^-(\text{aq}) + \text{SO}_3^-(\text{aq}) \rightarrow \text{S}_2\text{O}_6^{2-}(\text{aq})$ (R8)
	$\text{SO}_3^-(\text{aq}) + \text{SO}_3^-(\text{aq}) \rightarrow \text{SO}_3^{2-}(\text{aq}) + \text{SO}_3$ (R9)
Termination	$\text{SO}_3(\text{aq}) + \text{H}_2\text{O} \rightarrow \text{SO}_4^{2-}(\text{aq}) + 2\text{H}^+(\text{aq})$ (R10)
	$\text{SO}_4^-(\text{aq}) + \text{SO}_4^-(\text{aq}) \rightarrow \text{S}_2\text{O}_8^{2-}(\text{aq})$ (R16)
	$\text{SO}_5^-(\text{aq}) + \text{SO}_5^-(\text{aq}) \rightarrow \text{S}_2\text{O}_8^{2-}(\text{aq}) + \text{O}_2(\text{aq})$ (R17)



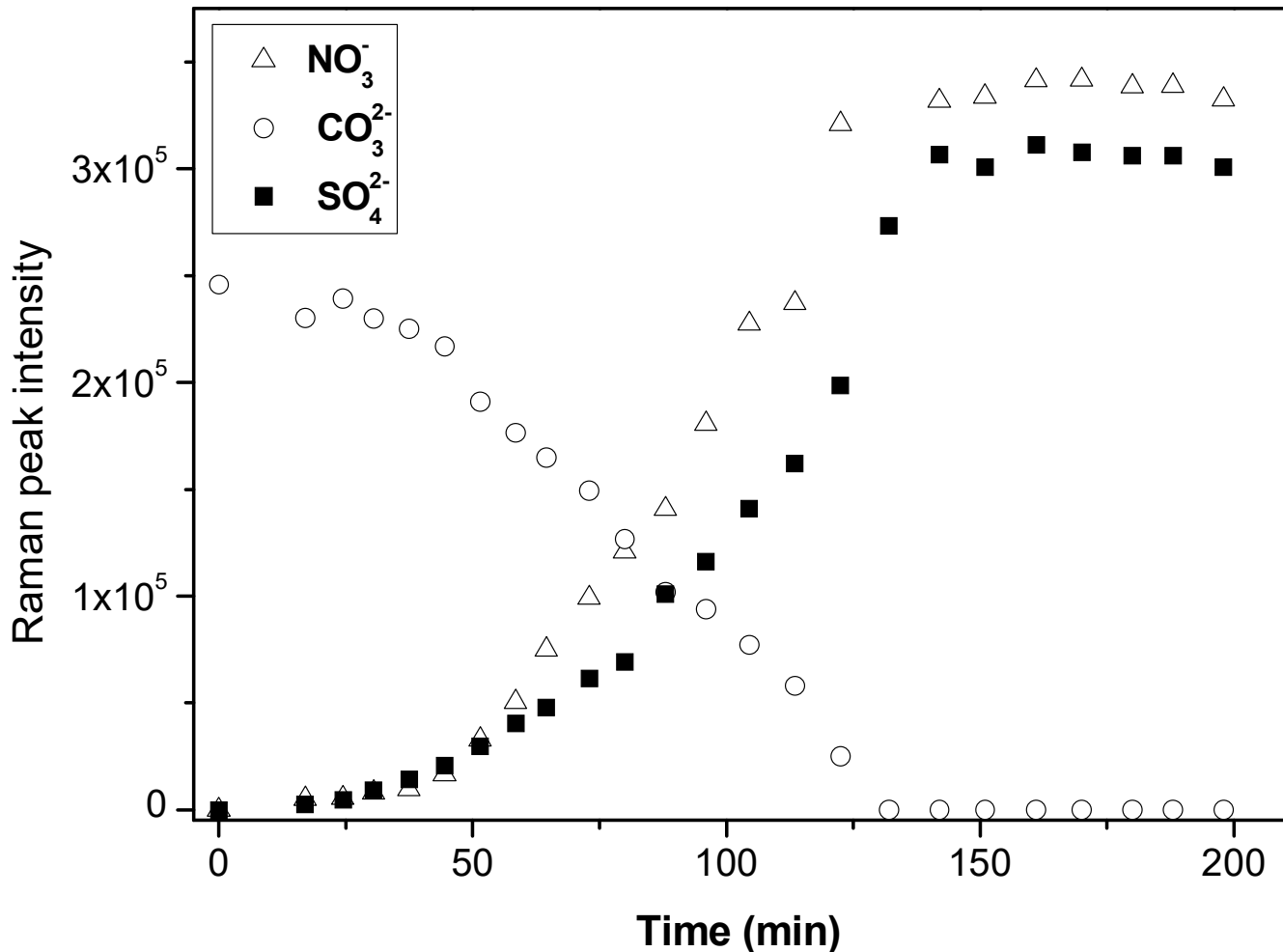
459
460 Figure 1. Raman spectra of a CaCO_3 particle during the multiphase reaction of SO_2 with $\text{O}_2/\text{NO}_2/\text{H}_2\text{O}$
461 on the particle. SO_2 : 75 ppm, NO_2 : 75 ppm, RH: 72%, O_2 : 20%. The peak intensity of carbonate (1087
462 cm^{-1}) at 0 and 42 min was divided by three for clarity.

463





470
 471 (iv)
 472 Figure 2. Microscopic image (i) and Raman mapping image of carbonate (ii), nitrate (iii), and sulfate (iv)
 473 on the CaCO_3 particle during the multiphase reaction SO_2 with $\text{O}_2/\text{NO}_2/\text{H}_2\text{O}$ on the particle. A-f
 474 corresponds to the reaction time of 0, 20, 41, 76, 117, and 193 min. SO_2 : 75 ppm, NO_2 : 75 ppm, RH:
 475 72%, O_2 : 20%. The mapping image of carbonate, nitrate, and sulfate are made using the peak area at
 476 1050, 1010, and 1087 cm^{-1} , respectively. The red, blue, and green colors indicate the peak intensity of
 477 carbonate, nitrate, and sulfate, respectively. The dashed lines in panel iii-f and iv-f indicate the shape of
 478 the droplet at the end of the reaction.
 479



480
481 Figure 3. Time series of the Raman peak intensity of NO_3^- , SO_4^{2-} , and CO_3^{2-} during the reaction of SO_2
482 with $\text{O}_2/\text{NO}_2/\text{H}_2\text{O}$ on CaCO_3 particles. SO_2 : 75 ppm, NO_2 : 75 ppm, RH: 72%, O_2 : 20%. The intensity of
483 NO_3^- , SO_4^{2-} , and CO_3^{2-} show the peak area at 1050, 1010, and 1087 cm^{-1} , respectively, in Raman spectra
484 obtained by Raman mapping.

485
486